Article

SYNTHESIS OF PALYGORSKITE PELLETS FOR APPLICATION IN ENVIRONMENTAL REMEDIATION

Karla Mayara Arguelles Simões[a,b,*], Giullia Bertrand Marçano[b,c], Fernanda Arruda Nogueira Gomes Silva[c], Luiz Carlos Bertolino[b], Maira da Costa de Oliveira Lima[d] and Lídia Yokoyama[a]

[a]Departamento de Processos Inorgânicos, Universidade Federal do Rio de Janeiro, 21941-909 Rio de Janeiro – RJ, Brasil

[b]Setor de Caracterização Tecnológica, Centro de Tecnologia Mineral, Ministério da Ciência, Tecnologia e Inovações (MCTI), 20941-908 Rio de Janeiro – RJ, Brasil

[c]Departamento de Química Inorgânica, Instituto de Química, Universidade Federal do Rio de Janeiro, 21941-909 Rio de Janeiro – RJ, Brasil

[d]Departamento de Engenharia Civil, Universidade Federal do Rio de Janeiro, 21941-804 Rio de Janeiro – RJ, Brasil

Received: 11/09/2023; accepted: 07/02/2024; published online: 08/30/2024

Palygoskite pellets were synthesized with lignin and WAX® and subjected to technological characterization for application in the remediation of Pb ions contained in aqueous effluents. X-ray diffraction (XRD) characterization of the palygorskite:lignin:WAX® material in a proportion of 70:15:15 revealed that the heat treatment of the pellets did not compromise the crystalline structure of the palygoskite. Texture analyses demonstrated that the surface area increased after synthesis and heat treatment, thus increasing the adsorption capacity. Regarding porosity, X-ray microtomography revealed that the pellets exhibit an irregular and porous spherical morphology with interconnected pores. Adsorption tests showed a removal of 73% of Pb^{II} contained in aqueous effluents after 15 min, with equilibrium reached in 60 min (88.36%). After the adsorption process, the presence of lead in the material was qualitatively confirmed through scanning electron microscopy and energy-dispersive X-ray spectroscopy (SEM-EDS) images. The produced pellets exhibit promising adsorbent qualities, such as strength and effective Pb^{II} ion adsorption.

Keywords: palygorskite pellets; pollution mitigation; heavy metal removal; water purification.

INTRODUCTION

Heavy metal contamination poses a serious threat to the environment and human health[1] due to its non-biodegradable nature and ability to bioaccumulate in the food chain.[2,3] To address this concern, researchers are focused on developing effective techniques for removing toxic metals from wastewater.[4] Various approaches, such as chemical precipitation, electrochemical processes, ion exchange, membrane filtration, and adsorption, are being explored for this purpose.[4] Adsorption stands out as a promising option due to its efficiency, low energy consumption, and reduced potential for secondary pollution. The search for economically viable alternatives remains a priority, aiming to apply this technology in both wastewater and soil treatment.[5]

Clay minerals have received attention as adsorbents for many environmental contaminants.[6-8] They are abundant, cheaper and environmentally friendly adsorbents[9] that can be used to substitute the expensive commercial activated carbon in remediation of environmental pollution.

Among them, palygorskite is a type of hydrated magnesium aluminum silicate minerals, which is composed of silicon dioxide as a tetrahedron and magnesium in an octahedral coordination.[10]

Its nontoxicity, good mechanical/thermal stability, low-cost and wide availability make it a potentially excellent adsorbent.

Although this clay mineral presents relevant adsorptive properties for the removal of metallic ions, such as lead, cadmium, chromium, nickel, and zinc,[11-14] the direct application of palygorskite in the adsorption of metals in aqueous effluents is hindered by the filtration stage of the processes due to the granulometry of the clay mineral (< 37 μm).

To overcome this challenge, agglomeration appears as a new alternative for this type of material. Agglomeration, also known as pelletization, converts fine powders into granular materials with controlled physical properties.[15,16]

Thereby, pelletizing consists of wet mixing fines with the addition of binders, followed by rolling in a disk or drum. Through the action of capillary surface tension, this promotes the formation of a spherical agglomerate. To enhance the physical and mechanical resistance of the formed pellets, a thermal treatment is conducted in a controlled atmosphere.[17] When this pellet is heated and water vaporizes, the pellet tends to disintegrate. Therefore, in order to prevent such effects, additives and binders are added aiming to improve the physical properties of the formed pellets. Generally, organic polymers are used as binders, in this sense, lignin is considered a promising binder due to its adhesive properties and its ability to agglomerate particles. It has a complex polymeric structure and can act as a binding agent when added to powdered materials, helping to form cohesive pellets or granules. Additionally, as lignin is an abundant by-product of the pulp and paper industry, its use as an organic binder also contributes to the valorization of industrial waste and the promotion of sustainability. WAX® is already widely used as a binder as it achieves good aggregability characteristics and has the advantage of fine particle size and being an inert material.

The pelletizing process for the aggregation of fine particles is mainly used for iron ores, however, for clay minerals it is little explored. The objective of this research was to characterize and assess the incorporation of lignin, a by-product of cellulose production obtained through the Kraft method, as well as WAX® binder, in the production of palygorskite pellets. Additionally, these pellets were utilized in an adsorption process aimed at the removal of Pb^{II}.

*e-mail: karla.carestiato@gmail.com

Associate Editor handled this article: Marcela M. Oliveira

EXPERIMENTAL

Materials, binder and mixture preparation

The raw palygorskite was obtained in Guadalupe, Piauí, Brazil, and its preparation was carried out as previously described by Simões *et al.*[18] In this study, palygorskite with a particle size below 20 μm was utilized.

The lignin sample (Klabin, Rio de Janeiro, Brazil) underwent a washing process in a vacuum filtration system and was subsequently dried in an oven at 40 °C for 30 h. It was then subjected to a grinding step using a basic analytical mill A11 (IKA, Guangzhou, China).

Micropulverized C-wax supplied by Merck (Darmstadt, Germany) and also known as WAX® binder, has the molecular formula $C_{38}H_{76}N_2O_2$ and molar mass of 593.03 g mol^{-1}. This binder did not require any prior treatment for use in the pelletizing process.

Palygorskite pellets: preparation and characterization

Palygorskite with a particle size below 20 μm was used for pelletization, employing both lignin and WAX® as binders. Tests were conducted with varying amounts (% m/m) of lignin and WAX® relative to the quantity of palygorskite. The systems created had the following compositions: 70:15:15, 80:10:10, and 60:20:20, denoting palygorskite:lignin:WAX® ratios. These mixtures were divided into quarters using a rotary fines splitter, model QRF-2 (CDC, São Paulo, Brazil), and subsequently further subdivided with a Rotary Micro Riffler sample (Quantachrome, Florida, USA).

The pellets were manufactured using a MSI Motor model SKR 63L (Madison Heights, USA) pelletizing disk equipped with a hard disk measuring 35 cm in diameter. The pelletizing procedure for palygorskite followed the method described by Campos and Fonseca,[17] with adjustments as described by Furlanetto.[19] These adaptations were necessary since the original procedures were designed for iron ore fines. During this process, sieves were employed to separate pellets of specific sizes, with smaller pellets being introduced into the disc feed to increase the overall mass. The following sieves were used: 6.35, 5.60, 4.75, 3.36, 2.80, and 1.68 mm in opening size, and the chosen size range fell between greater than 3.36 mm and less than 4.75 mm.

Following this procedure, the pellets were spread out on trays and allowed to dry for 24 h at room temperature. Subsequently, they were placed in an oven at a temperature of approximately 60 °C for further drying.

Heat treatment

The heat treatment of the pellets was conducted in a muffle furnace, model LF0061201 (Jung, Florida, USA). Pellets falling within the size range of 2.80 to 4.75 mm were carefully chosen, and approximately 3 to 4 g of these pellets were weighed and placed into small porcelain boats. These boats were then introduced into the muffle furnace and exposed to temperatures of 100, 200, and 300 °C for varying durations of 30, 60, and 90 min.

Subsequently, the heat-treated pellets, denoted as PLW_HT, underwent characterization using a range of techniques, including X-ray diffraction (XRD), N_2 physisorption, scanning electron microscopy (SEM), Zeta potential analysis, contact angle and computed microtomography.

X-Ray diffraction (XRD)

XRD patterns of the samples were obtained using the powder method with a Bruker D4 Endeavor equipment (Massachusetts, USA). The X-ray source used was Co Kα radiation at 35 kV/40 mA. The goniometer operated at a velocity of 0.02° (2θ) *per* step with a 1 s collection time *per* step, and data were collected in the range of 5 to 80° (2θ).

To qualitatively interpret the obtained spectra, a comparison was made with standards available in the PDF02 database (ICDD 2006), and this analysis was performed using the Bruker AXS software DiffracPlus (Massachusetts, USA).

Textural properties

The textural properties of the mixture composed of palygorskite, lignin, and WAX®, as well as the untreated pellets (PLW_WT) and heat-treated pellets (PLW_HT), were determined through nitrogen (N_2) physisorption analysis conducted at –196 °C (77 K). These analyses were carried out using a Micrometrics instrument (Georgia, USA), with approximately 400 mg of each sample.

Prior to the actual analysis, a pretreatment step was performed on the samples. This pretreatment involved drying the samples at 100 °C under a vacuum of 1×10^{-6} mmHg for 24 h to eliminate physically adsorbed water. Following the pretreatment, the analysis involved obtaining adsorption and desorption isotherms by varying the partial pressure of N_2. From these isotherms, the surface area was calculated using the BET (Brunauer, Emmett and Teller) method, and the pore size distribution was determined from the desorption isotherm of N_2 using the BJH (Barret-Joyner-Halenda) method.

Scanning electron microscopy (SEM)

Scanning electron microscopy analysis was conducted using a Hitachi TM303 Plus microscope (Tokyo, Japan) equipped with modules for secondary electrons, backscattered electrons, and energy dispersive X-ray spectrometry (EDS). This analysis aimed to qualitatively determine the chemical elements present in the samples.

To prepare the samples for SEM analysis, they were metallized with silver using the Bal-Tec-SCD005 Sputter Coater equipment (Uzwil, Switzerland). Metallization with silver is a common technique used in SEM to enhance the conductivity of non-conductive samples and improve image quality during analysis.

Zeta potential

The Zeta potential, which represents the surface charge of lignin, was determined using the Zetasizer Nano ZS equipment (Malvern, United Kingdom). To perform the measurements, 0.5 g of sample solutions were prepared in 10 mL of KCl with a concentration of 10^{-3} mol L^{-1}, serving as the electrolyte.

For pH adjustment in the range of 1.5 to 11.0, HCl or KOH solutions were used, and this adjustment process was facilitated by employing a potentiometric titrator coupled to the system.

Contact angle

The procedure was conducted after calibrating the MSA One-Click SFE mobile surface analyzer (Krüss, Hamburg, Germany), using an acrylic surface. Duplicate measurements of contact angles were taken for manually added droplets. The parameters used included a temperature of 20 °C, an aliquot volume of 2 μL, water-based solvent, and the double sessile drop method. For the sample analysis, it was necessary to use two supports to maintain the equipment at a standard height, ensuring stability during the procedure.

X-Ray microtomography

Microtomography images were acquired with a cone beambenchtop X-ray microCT scanner from SkyScan, model 1172 (Bruker, Massachusetts, USA). Table 1 outlines the imaging conditions employed for capturing images of the PLW_HT sample. To assess pore connectivity, a minimum threshold of 10,000 pixels was applied to identify clusters within the images.

Table 1. Parameters for image acquisition through computerized microtomography

Parameter	Value
Source voltage / kV	120
Current / mA	100
Distance from source to detector / mm	820
Resolution / μm	3.5
Number of frames	2878

Adsorption tests

The adsorption efficiency of the produced pellets was assessed through batch experiments using a lead(II) nitrate ($Pb(NO_3)_2$) solution. These experiments involved utilizing 0.5 g of pellets and 20 mL of the lead solution, with a contact time of 1 h. To facilitate contact between the pellets and the effluent, agitation was carried out using an orbital shaking table, model KS 4000i, (IKA, Guangzhou, China), with a rotation speed of 100 revolutions *per* minute (rpm) at room temperature.

The tests were conducted in duplicate to ensure reliability, and the quantification of lead ions after adsorption was performed using atomic absorption spectroscopy.

Quantification of Pb^{2+} ions

The analytical method employed for determining the total concentration of Pb^{2+} ions dissolved in synthetic effluent was inductively coupled plasma optical emission spectrometry (ICP-OES). The analyses were conducted using equipment from Horiba Jobin Yvon (Longjumeau, France).

To study the lead adsorption isotherm and comprehend the relationship between the effluent concentration and the quantity of Pb^{2+} ions adsorbed, the adsorption capacity (q_e) and removal percentage (R%) of palygorskite pellets at equilibrium were calculated using the Equations 1 and 2:

$$q_e = \frac{(C_0 - C)V}{m} \quad (1)$$

where: q_e is the adsorption capacity, C_0 is the initial concentration of Pb^{2+} ions in the effluent, C_e is the equilibrium concentration of Pb^{2+} ions in the effluent, V is the volume of the effluent, m is the mass of palygorskite pellets used.

$$R(\%) = \frac{(C_0 - C)}{C_0} \times 100 \quad (2)$$

where: R% is the removal percentage, C_0 is the initial concentration of Pb^{2+} ions in the effluent, C_e is the equilibrium concentration of Pb^{2+} ions in the effluent.

These equations allow you to determine the adsorption capacity and the percentage of lead ions removed by the palygorskite pellets in equilibrium with the effluent.

Influence of contact time

To investigate the influence of contact time on the adsorption process of lead ions in batch experiments, samples were analyzed at various time intervals, specifically: 15, 30, 45, 60, 75, 90, and 120 min. The initial concentration of the $Pb(NO_3)_2$ solution was set at 77.3 mg L^{-1}, and the experimental parameters remained consistent with those described in the preliminary test mentioned in the previous topic. This analysis helps in understanding how the adsorption of lead ions by the palygorskite pellets evolves over time.

Influence of metal ion concentration

The influence of the concentration of lead(II) metal ions was investigated as it plays a crucial role in the adsorption rate. This variable is of paramount importance for understanding the adsorption process, as it is typically used to determine the maximum adsorption capacity of the metal ion by the chosen adsorbent. Table 2 presents the experimental conditions employed during the study. Following the completion of the test, the solution was subjected to atomic absorption analysis to quantify the concentration of Pb^{II} ions.

Table 2. Fixed parameters to evaluate the influence of metal ion concentration

Parameter	Value
Mass of adsorbent / g	0.5
Initial concentration of metal ion / (mg L^{-1})	30.9, 54.4, 148.0, 217.0, 312.0, 426.0, 517.0, 643.0, 801.0, 907.0 and 1049,0
Temperature / °C	25
Agitation / rpm	100
Time / min	60

The results of the adsorption tests conducted to remove $Pb(NO_3)_2$ were used to create the adsorption isotherm. The data obtained from these tests were then fitted to Langmuir and Freundlich models, which are commonly used to describe adsorption processes and provide insights into the adsorption behavior of the material being studied. These models help in understanding how adsorbents interact with adsorbates and provide valuable information about the adsorption capacity and mechanisms.

Langmuir isotherm

This model assumes that the surface is energetically homogeneous, all adsorption sites are equally active and surface coverage occurs in a monolayer without interaction between the adsorbed molecules.[20] The model for single-component systems is described in Equation 3.

$$q_e = \frac{q_m K_L C_e}{1 + K_L C_e} \quad (3)$$

where: q_e (mg g^{-1}) is the adsorptive capacity at equilibrium; Q_m (mg g^{-1}) is the maximum adsorptive capacity; K_L (L mg^{-1}) is the Langmuir equilibrium constant, representing the affinity between the adsorbent and adsorbate, C_e (mg L^{-1}) is the adsorbate concentration at equilibrium.

The separation factor R_L (dimensionless) can be expressed as described by Hall *et al.*,[21] as shown in Equation 4:

$$R_L = \frac{1}{1 + K_L C_0} \quad (4)$$

here, C_0 (mg L^{-1}) is the initial adsorbate concentration.

The value of R_L helps determine the nature of the adsorption isotherm:

If $R_L > 1$, it indicates unfavorable adsorption.

If $0 < R_L < 1$, it indicates favorable adsorption.

If $R_L = 1$, it indicates linear adsorption.

If $R_L = 0$, it indicates irreversible adsorption.[22]

Freundlich isotherm

The Freundlich model was first described by Max Finley Freundlich in 1906. This empirical model can be used in non-ideal systems, that is, it portrays heterogeneous surfaces, in which the active

sites have different energies and multilayer adsorption, characteristic of a physisorption process.

The non-linear form of the Freundlich model is presented in Equation 5. The linear form, obtained by applying log in the non-linear form, is presented in Equation 6, which allows determining the parameters K_F and n from the linear and angular coefficients of the line obtained when plotting the $\log q_e \times \log C_e$ graph.

$$q_e = K_F C_e^{1/n} \quad (5)$$

$$\log q_e = \log K_F + \frac{1}{n} \log C_e \quad (6)$$

where: q_e (mg g^{-1}) represents the adsorptive capacity at equilibrium, K_F (L mg^{-1}) is the Freundlich constant, indicating adsorption capacity, C_e (mg L^{-1}) is the adsorbate concentration at equilibrium, n (dimensionless) is the Freundlich exponent or heterogeneity factor, which reflects the intensity of adsorption.

The adsorption process can be evaluated from the value of the affinity constant n, which values between 1 and 10 are characteristic of a favorable adsorption process.[23]

Characterization after the adsorption process

The pellets after the lead ion adsorption process were characterized using the SEM-EDS, already described in "Scanning electron microscopy (SEM)" sub-section.

RESULTS AND DISCUSSION

Influence of the amount of binder

To assess the impact of the binder content in the created systems, three distinct proportions were examined, specifically: 70:15:15, 80:10:10, and 60:20:20, representing palygorskite:lignin:WAX ratios, respectively.

In the case of the 80:10:10 proportion, it is important to note that no pellets were formed. This outcome can be attributed to the relatively low quantity of binders used. In this particular ratio, the mass of lignin used in conjunction with WAX® was insufficient for the successful formation of pellets. This observation underscores the critical role of binders in pellet formation, and insufficient binder content can hinder the desired pelletization process.

In the case of the 60:20:20 proportion, some pellets were formed with smaller sizes. However, this proportion is also not adequate. The limited pellet formation may be attributed to the high quantity of WAX® in the system, as it has low solubility in water, which can affect the pelletization process.

For the 70:15:15 ratio, the most favorable pellet formation was observed, both in terms of size and quantity. Notably, smaller pellets that were produced were reintroduced into the pelletizer disc to achieve the desired mass and shape. This was achieved by employing a series of sieves with varying opening sizes: 6.35, 5.60, 4.75, 3.36, 2.80, and 1.68 mm for the classification of the formed pellets.

In summary, to carry on with the study, all subsequent tests were conducted using the 70:15:15 ratio, as it yielded the most favorable results for pellet formation. This decision was based on the superior performance in terms of pellet size and quantity.

Heat treatment

The purpose of subjecting the pellets to thermal treatment was to enhance their resistance, especially since they exhibited some disintegration after just 5 min. The selection of temperatures for this treatment was based on the thermogravimetry/derivative thermogravimetry (TG-DTG) analysis of the palygorskite from the same mine, as characterized by Simões *et al.*[18] Importantly, these temperatures were chosen to ensure they would not compromise the structure of the clay mineral. In fact, within this temperature range, there is an improvement in the adsorptive properties due to the removal of physically adsorbed water on the surface of palygorskite as well as water present in its channels.

In a study carried out by Maciel *et al.*,[24] a heat treatment of up to 100 °C for 1 h was performed on palygorskite pellets, cement, and WAX®. The results indicated that there was an increase in surface area, volume, and pore size, although not very significant, as measured by BET analysis.

The thermal treatment proved to be effective in terms of enhancing the resistance of the pellets to the medium, as they did not disintegrate even after 24 h of contact with an aqueous solution. This suggests that the treatment successfully stabilized the pellets, making them more durable for the desired application.

Based on the observations from the water solubility test, it became evident that the pellets subjected to heat treatment at 300 °C for 30, 60, and 90 min in a muffle furnace exhibited the highest resistance to the aqueous medium. However, it was also noted that in the pellets treated for 30 and 60 min, some parts of the lignin were not completely burned, as indicated by the brown discoloration. Over time, these pellets started to disintegrate.

As a result, it was decided to carry out the entire study of the adsorptive process using pellets that had been treated at 300 °C for 90 min. These pellets demonstrated superior resistance to the aqueous medium and did not exhibit the issues observed in the shorter treatment times.

The use of X-ray diffraction allowed the identification of the mineralogical phases present in the sample. It was observed that the heat treatment conditions did not lead to the collapse of the clay mineral structure. In the PLW_HT sample, characteristic peaks corresponding to various minerals were identified: palygorskite ($(MgAl)_5Si_8O_{20}(OH)_2(OH_2)_4.4H_2O$) at 9.77° (2θ), quartz (SiO_2) at 31.05° kaolinite ($Al_4(Si_4O_{10})(OH)_8$) at 14.33° and illite at 40.90°, these three minerals being considered impurities contained in the samples. This mineralogical composition is similar to that of other palygorskite samples from the same region of Guadalupe (PI, Brazil) and is consistent with findings in the existing literature.[18,25]

As depicted in Figure 1S (Supplementary Material), the heat treatment conditions applied at 300 °C for 90 min did not result in the collapse of the palygorskite structure. Consequently, the adsorptive properties of the material were preserved, validating its suitability for the intended applications.

Table 3 provides an overview of the textural properties of the mixture composed of palygorskite, lignin, and WAX®, along with the pellets both before and after heat treatment. These properties play a crucial role in understanding the characteristics of the material and suitability for applications in adsorption process.

Based on the data obtained, it is possible to observe that the pelletizing process reduces the surface area of the system, which

Table 3. Texture properties of untreated and thermally treated palygorskite:lignin:wax pellets and palygorskite:lignin:wax powder mixture

Sample	Surface area / (m^2 g^{-1})	Average pore size / Å	Average pore volume / (cc g^{-1})
Mixture (PLW)	7.072	19.479	0.087
PLW_WT	1.033	15.555	0.009
PLW_HT	14.690	19.646	0.105

PWL: palygorskite:lignin:WAX; PLW_WT: untreated pellets; PLW_HT: heat-treated pellets.

was expected, as literature typically reports values ranging from 125 to 210 $m^2 g^{-1}$.[26] However, after the heat treatment, an increase in the surface area of the formed pellets was observed. This increase can be associated with the removal of water present in the palygorskite channels, as well as promoting a better interaction of organic materials with the clay mineral, resulting in a new configuration of palygorskite aggregates and clusters, due to the possibility of accommodating organic compounds that previously did not exist, and consequently contributing to the increase in surface area and pore volume. When combined with lignin and WAX, palygorskite demonstrated compatibility, resulting in high pore connectivity, as will be shown later, and physical strength, remaining aggregated throughout the adsorptive process. Therefore, it is evident that the heat treatment performed was effective not only in terms of material durability but also in enhancing the adsorption capacity of the pellets.

Regarding the average pore size, it is possible to classify the material as mesoporous according to the International Union of Pure and Applied Chemistry (IUPAC) classification, which covers the range from 2 to 50 nm. This classification holds true for all samples, as the largest pore size distribution falls within this range. In mesoporous materials composed of a combination of organic and inorganic components, the adsorption of metal ions can occur both on the external surface, where functional groups facilitate direct adhesion (internal sphere), and within internal pores and cavities, retaining the ions (external sphere). It is believed that both mechanisms may coexist and influence the adsorption of heavy metals.[27]

The Zeta potential graph associated with pH for the PLW_HT sample demonstrates that the formed pellets have a predominantly negative surface charge within the examined pH range (Figure 2S, Supplementary Material). Additionally, as pH increases, the surface charge becomes increasingly negative. This observation is significant as it promotes the adsorption of positively charged ions, such as lead(II) ions.

The average contact angles of the evaluated regions ($R1_{average} = 69.1$ and $R2_{average} = 67.85°$) indicate a better propensity for the liquid to spread and wet the solid surface. The adsorption of metal ions is influenced by both the surface area and its water-wettability capacity. Materials with hydrophilic surfaces, low contact angles, and high surface energy have higher efficacy in adsorbing heavy metals in aqueous solution due to their greater affinity and interaction capacity with the metal ions.[28]

Based on the X-ray microtomography represented in Figure 1, it is evident that the material exhibits a porous nature, as anticipated, given that the sample comprises 70% palygorskite. Furthermore, the irregular spherical shape of the produced pellets is also noticeable, which presents a challenge in selecting the analysis region for segmentation. This, in turn, poses an obstacle to conducting quantitative analysis of the pore volume in the samples. It is crucial to emphasize that this image is merely a snapshot captured during the three-dimensional study.

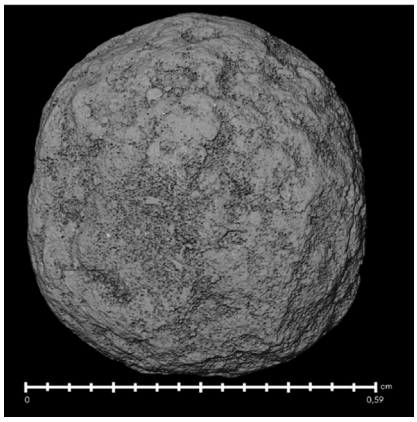

Figure 1. *Microtomography of the PLW_HT sample*

Figure 2a clearly shows that the entire selected region is contained within the sample. In Figure 2b, it is evident that the connectivity of the pores is higher than what was observed in the scanning electron microscopy analysis. Additionally, it is apparent that the pores exhibit irregular shapes, and the images reveal the presence of various mineralogical phases within the sample. Notably, minerals with higher attenuation correspond to the white color in the image (Figure 2c), while quartz exhibits an intermediate gray coloration, and the pores are depicted in black.

The sample photograph includes a representative illustration of the selected volume used for processing the presented data (Figure 3a). To calculate the pore volume, a mesh was created to account for the imperfect sphere shape and ensure that all the pellet was included in the quantification, as illustrated in Figure 3b. The analysis revealed that the porosity of the heat-treated palygorskite, lignin, and WAX® pellets is approximately 15%. Figure 3b depicts the 3D representation of the sample pores, highlighted in blue.

The microtomography treatment enables the visualization of the inherent pore connectivity within the samples, as demonstrated in Figures 4a and 4b for the PLW_HT sample.

Note in the images that several clusters are forming through interconnected pores. Each color in the cluster identifies pores that are connected to each other but not to clusters of a different color. Therefore, it can be concluded that these pellets exhibit well-connected pore spaces. It is worth highlighting the presence of spheres in the PLW_HT sample (Figure 4a). These spheres may be attributed to the agglomeration of particles that compose the pellets, facilitated

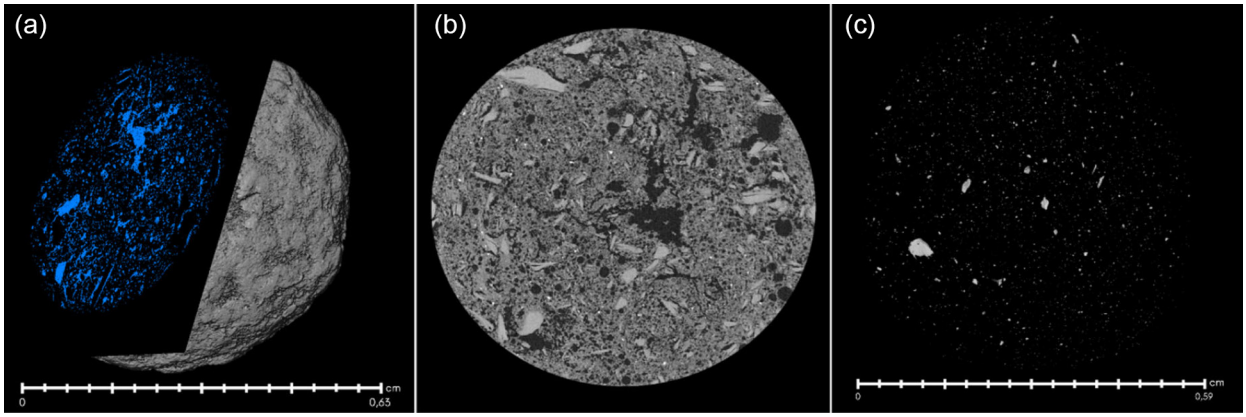

Figure 2. *Microtomography of the PLW_HT sample: (a) selection region; (b) overview of pore connectivity; (c) mineralogical phase*

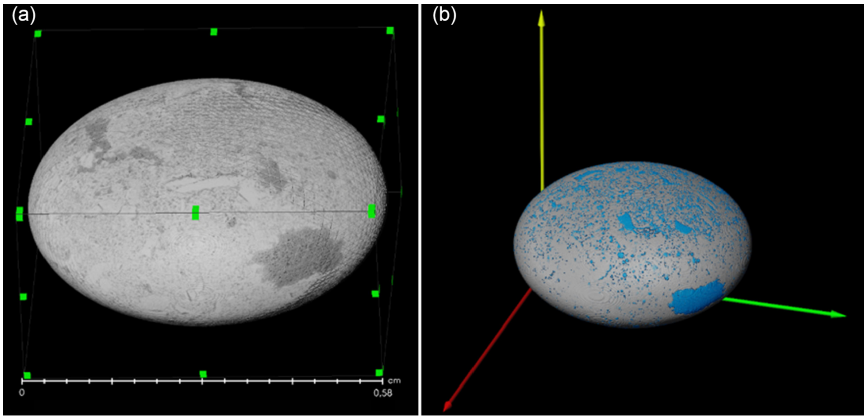

Figure 3. *Sample with mesh to select area for volume calculation and 3D connectivity of pellets_HT*

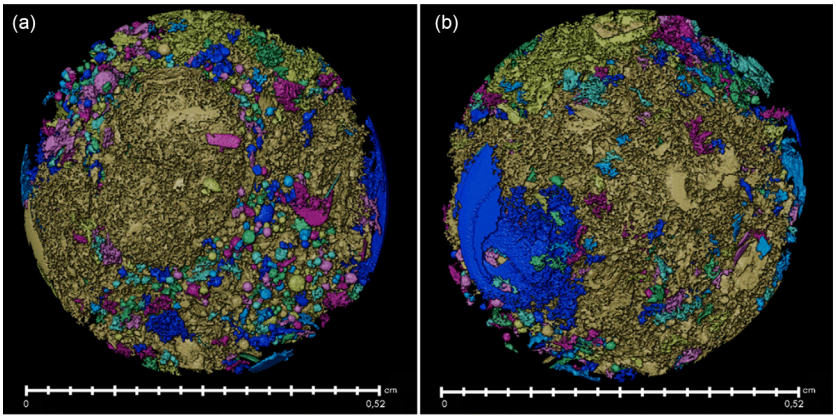

Figure 4. *Pore connectivity of the PLW_HT sample using micro-CT*

by the action of binders, resulting in the formation of smaller spheres within the material.

Adsorption of lead ions in batch process

Influence of time on the adsorptive process

Kinetic parameters play a crucial role in sorption processes as they help predict the adsorption rate and provide essential information for process modeling. Consequently, the kinetics of adsorption for the removal of Pb^{II} was examined and interpreted using pseudo-first-order and pseudo-second-order kinetic models.[29]

Based on the results obtained in the adsorption study, it is clear that contact time plays a significant role in the process efficiency. Remarkably, within just 15 min, there was a removal of approximately 73% of lead(II) ions from the solution. Subsequently, after 90 min, the adsorption percentage remained nearly constant, indicating the equilibrium point for the process.

Between 75 and 120 min, the highest adsorption percentage, approximately 96%, was observed, albeit with some pellets undergoing disaggregation during this period. This led to an increase in surface area and consequently enhanced removal efficiency in the adsorption process. Hence, we selected a 60 min duration, where the removal percentage was 88.36%, as the equilibrium time for the adsorption process in this study, indicating the saturation of the pellets (the adsorbent material used).

The rapid attainment of adsorption equilibrium indicates that the adsorbent surface is readily available for adsorption. Consequently, the observed effect of contact time suggests a significant increase in adsorption within the initial minutes of contact between the adsorbent and the metal ion. Similar trends have been reported in the literature.[11,14] For instance, Potgieter *et al.*[11] conducted a study on the effect of time for the removal of Pb^{II} using powdered palygorskite as an adsorbent and concluded that equilibrium is reached rapidly, typically within just 30 min. This finding further supports the notion that the adsorption sites are well-exposed and readily accessible.

According to a study conducted by Simões,[14] in 2023, where the equilibrium time was exclusively examined using powdered palygorskite for the removal of lead(II) ions, it was observed that there was no significant variation in the percentage of adsorption within the time interval ranging from 10 to 360 min. Considering that the palygorskite used in this current work has also been enhanced and that the surface area of the powdered sample is notably higher compared to the pellet samples, it was anticipated that there might be a reduction in the percentage of adsorption when using pellets, in line with the observations made.

Considering that powdered palygorskite is an excellent adsorptive material, known for its high metal ion removal efficiency, it faces a limitation in direct application due to its fine granularity. However, the results obtained from adsorption using pellets made from this material are promising. This opens up the possibility of applying the material in adsorption columns.

Utilizing a fixed bed column for adsorption offers several advantages, including the ability to carry out the process continuously without interruptions until the adsorbent becomes saturated. Additionally, to enhance the efficiency of the process, it is feasible to use the pellets as adsorbents in series columns.

Kinetic data were analyzed using two kinetic models: pseudo-first order and pseudo-second order. The kinetic models were linearized using Equations 7 and 8, respectively.

$$\ln(q_e - q_t) = \ln q_e - k_1 t \quad (7)$$

$$\frac{q_t}{t} = -(k_2 q_e) q_t + k_2 q_e^2 \quad (8)$$

where: q_e (mg g^{-1}) is the adsorption capacity *per* gram of adsorbent at equilibrium; q_t (mg g^{-1}) is the adsorption capacity *per* gram of adsorbent at time t; t (h) is the contact time; k_1 (h^{-1}) is the pseudo-first order adsorption rate constant; k_2 (g mg^{-1} h^{-1}) is the pseudo-second order adsorption rate constant.

The values obtained for the adsorption capacity at equilibrium, as well as the adsorption rate constant and the correlation coefficient (R^2) for each of the linearized models are presented in Table 4.

Table 4. Fit parameter values determined by linearized kinetic models

Model	Parameter	Value
Pseudo-first order	k_1 / (h^{-1})	0.0318
	q_e / (mg g^{-1})	0.9687
	R^2	0.987
Pseudo-second order	k_2 / (g mg^{-1} h^{-1})	0.0457
	q_e / (mg g^{-1})	3.1162
	R^2	0.9993

q_e: adsorption capacity *per* gram of adsorbent at equilibrium; k_1: pseudo-first order adsorption rate constant; k_2: pseudo-second order adsorption rate constant; R^2: correlation coefficient.

Based on the results analysis, it is observed that the correlation coefficients (R^2) of the pseudo-second-order kinetic model for Pb^{II} are higher than those obtained with the pseudo-first-order model. The pseudo-second-order model exhibits superior correlation coefficients with the experimental data (R^2 = 0.9993), indicating that this model provides a better description of the kinetics of the process.

While the pseudo-first-order model also yields a reasonable R^2 value, it results in an adsorption capacity value of 0.9687 mg g^{-1} of adsorbent at equilibrium. This value significantly deviates from the experimental q_e value (2.73 mg g^{-1}).

In the case of data adjustment for the pseudo-second-order model, not only is the R^2 value higher, but also the calculated value of q_t (3.1162 mg g^{-1}) is closer to the experimentally determined value (2.73 mg g^{-1}). Additionally, the adsorption rate constant for the process is determined to be 0.0457 g mg^{-1} h^{-1}.

This model suggests that the adsorption rate depends on the quantity of ions on the surface of the adsorbent and the amount of ions adsorbed at equilibrium, taking into consideration the active sites of the adsorbent and the concentration of metal ions.

Influence of metal ion concentration on the adsorptive process

The initial concentration of metallic ions is a crucial variable influencing the performance and efficiency of the adsorption process. As noted by Demey *et al.*,[30] increasing the concentration of the metal ion progressively enhances the removal of the metal until it reaches a saturation level.

Modeling, in conjunction with the analysis of equilibrium data, enables the development of adsorption isotherms, which are pivotal in translating laboratory results into practical applications. These isotherms aid in comprehending process mechanisms, analyzing experimental data, predicting responses under operational conditions, and optimizing the process.[31]

Figure 5 depicts the adsorption isotherm of metallic cations, specifically Pb^{II}. On the ordinate axis, the quantities of the adsorbed ions *per* unit mass of the adsorbent (q_e) are plotted, while the abscissa axis represents the concentration of Pb^{II} in solution after equilibrium (C_e). The experiments were conducted within an initial concentration range spanning from 30.9 to 1049.0 mg L^{-1} while maintaining the other parameters constant.

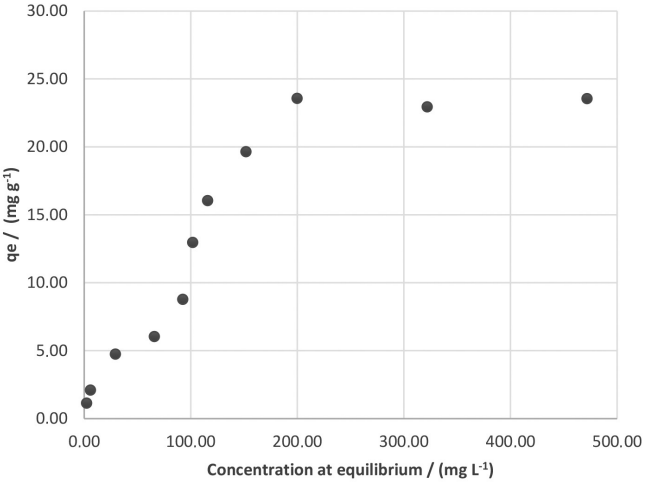

Figure 5. *Adsorption isotherm as a function of the equilibrium concentration of Pb^{II}*

The profile of this isotherm illustrates that the adsorption process for lead ions using the pellets is favorable for extracting relatively high amounts, even at low levels of adsorbate concentration in the fluid. Furthermore, it is evident that a plateau is formed, indicating an approach to equilibrium, consistent with the types of isotherms described by McCabe *et al.*[32] It can be observed from Figure 5 that, for an initial metal ion concentration of 1049.00 mg L^{-1}, the q_e value obtained was 23.55 mg g^{-1} of Pb^{II}.

The adsorption isotherms can be categorized into four groups based on the shape of the curve. From the graph presented in Figure 5, it can be inferred that the isotherm obtained for the palygorskite pellets in the Pb^{II} adsorption process falls within class L and subgroup 4.[33] Isotherms in this class suggest that as more solid sites are occupied during the process, it becomes increasingly challenging for other solute molecules to occupy vacant sites, leading to the initial downward curvature. Furthermore, it indicates that molecules are adsorbed in layers, which is characteristic of subgroup 4. This suggests that adsorption occurs in a horizontal manner with limited competition from the solvent for surface sites.

In this context, numerous models have been developed to describe isotherms, and they have proven to be successful in explaining the sorption mechanism.[34] Despite being empirical models with straightforward mathematical relationships, typically characterized by the number of adjustable parameters, they generally offer a sound representation of experimental behavior across a broad range of operating conditions.[31,35]

Langmuir isotherm

The Langmuir isotherm is based on three key assumptions: first, that sorption is limited to monolayer coverage; second, that all surface sites are identical and can only accommodate one adsorbed atom; and third, that the ability of a molecule to be adsorbed at a given location is independent of its occupation. According to the Langmuir model, the saturation capacity (q_{max}) must correspond to the saturation of a fixed number of identical surface sites, representing the equilibrium distribution of metal ions between the solid and liquid phases. This model assumes uniform adsorption energies at the surface and no transmigration of the adsorbate in the surface plane.[21]

Fittings of lead adsorption data to the linearized equation of the Langmuir model are shown in Figure 6.

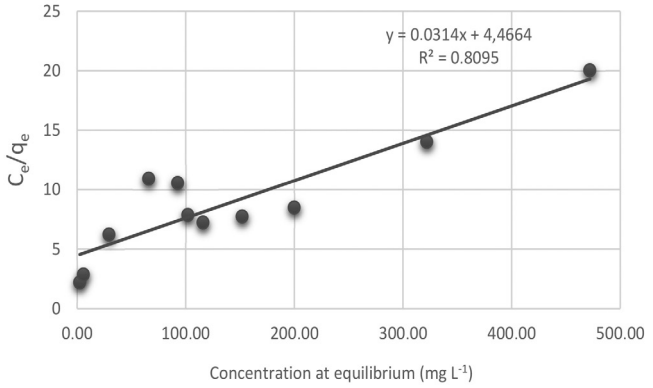

Figure 6. *Adsorption isotherm for lead ions linearized using the Langmuir model*

Based on the data fitting, the maximum adsorption value (q_m) was determined to be 31.84 mg g^{-1}, with a value of b equal to 0.0070 and an R^2 of 0.8095. In a similar data fitting conducted by Simões *et al.*,[14] using processed palygorskite, the Langmuir model achieved an R^2 of 0.9943. It is worth noting that in the study conducted by Potgieter *et al.*[11] on lead ion adsorption, it was reported that the adsorption profile of palygorskite is well described by the Langmuir equation.

Freundlich isotherm

Developed with the primary objective of empirically studying the adsorption of gases on solid surfaces,[36] the Freundlich model, similar to the Langmuir model, has found extensive application in describing the adsorption of metal ions using various adsorbents.

Primarily employed to characterize adsorption on heterogeneous surfaces,[37] this model assumes that sites with higher binding affinities are occupied first.[38]

Fitments of lead adsorption data to the linearized equation of the Freundlich model are presented in Figure 7.

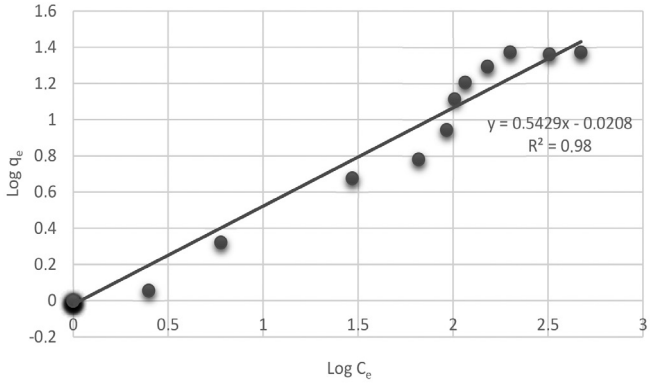

Figure 7. *Adsorption isotherm for lead ions linearized using the Freundlich model*

The parameters of the Freundlich isotherm, K_F and n, are respectively determined from the intercept and slope of the line generated by plotting log q_e *versus* log C_e. Based on the data fitting, the values of n, K_F, and R^2 were found to be 1.84, 1.04, and 0.98, respectively.

The n parameter signifies how the adsorption sites are distributed in terms of their energy. According to Freitas *et al.*,[39] when n is greater than 1, as is the case for lead adsorption in this study, it indicates that these sites are energetically heterogeneous.

Due to the addition of binders in the clay mineral pelletizing process, the pelletized palygorskite (palygorskite, WAX® and lignin) becomes a heterogeneous adsorbent. As noted by Aguiar *et al.*,[40] a higher value of n indicates greater heterogeneity of the adsorption sites.

When comparing the R^2 values of the Langmuir and Freundlich isotherms, it is evident that the Freundlich isotherm (R^2 = 0.98) provides a better fit to the data, as previously anticipated. This improved fit can be attributed to the presence of binders, particularly lignin, which, as indicated by surface charge measurements (Zeta potential), carries a negative charge. This negative charge promotes the adsorption of metallic cations.

The suitability of the Freundlich model for pelletized palygorskite was also observed by Furlanetto,[19] who obtained a value of n equal to 1.29 and K_F = 0.87 L $mmol^{-1}$ with an R^2 of 0.9905.

Compliance to the Freundlich model does not necessarily characterize a unique process, such as physisorption, but suggests that the adsorbed may bind to chemically diverse sites of a heterogeneous adsorbent. This observation aligns with findings by Furlanetto.[19] Consequently, the available surface sites on the material for the adsorption of lead(II) ions are not uniformly distributed in terms of energy, as it is a heterogeneous composite.

Guo *et al.*[41] investigated the adsorption of metal ions on lignin isolated from black liquor. Their study revealed the affinity of lignin for various types of metallic cations, with the order of affinity presented as follows: $Pb^{II} > Cu^{II} > Cd^{II} > Zn^{II} > Ni^{II}$. Furthermore, through surface complexation modeling, it was evident that the lignin surface contains two main types of acidic sites attributed to carboxylic and phenolic surface groups. Among these, the phenolic sites exhibited a higher affinity for metal ions compared to the carboxylic sites.

Chen *et al.*[42] conducted a study on the adsorptive process of cations, including Pb^{II}, using Kraft lignin. Lignin exhibited a significant affinity for the adsorption of lead ions, reaching approximately 49.8 mg g^{-1} of lignin. This study also revealed that the adsorptive process could be reversed by adjusting the pH, further highlighting the potential of lignin for such applications.

Pellet characterization tests after the adsorption process

The palygoskite, lignin and WAX® pellets after the lead ion adsorption process were analyzed by SEM-EDS and surface charge measurements (Zeta potential). The characterization techniques used confirmed the presence of the metal on the surface of the clay mineral after the adsorption process.

Scanning electron microscopy and energy dispersive X-ray spectrometry (SEM and EDS)

The images captured by scanning electron microscopy suggest the presence of denser elements at certain points of the sample, as indicated by the white dots in Figure 3S (Supplementary Material). Figure 3S displays a clustering of these elements, which, through energy dispersive X-ray spectrometry (EDS), confirmed the presence of lead. In Figure 4S (Supplementary Material), the EDS analysis of the pellet samples after the adsorption process reveals the presence of lead in the examined region. Furthermore, it is qualitatively evident that a significant amount of lead is present in the highlighted region, while other areas are associated with palygorskite. In another region of the sample (Figure 5S, Supplementary Material), where the presence of lead was also identified, mapping was conducted to corroborate the aforementioned findings. Through this analysis, the distribution of elements across the entire examined area can be observed, as visualized in Figure 5S. In this mapping, the blue color represents the magnesium element, characteristic of palygorskite, while the red color is associated with lead, whose presence on the material surface is evident in the light color observed.

Prospective future research

Based on the results obtained for different concentrations of Pb^{II}, it is imperative to assess the compression resistance of the pellets and implement their application in a fixed bed column system, while also conducting a kinetic study of the process. Furthermore, it is essential to investigate the desorption process to determine the feasibility of reusing the adsorbent in subsequent processes.

CONCLUSIONS

The pelletization process and thermal treatment proved to be highly efficient, enabling the production of pellets with the required strength and properties for use in the adsorption process. These pellets were manufactured using lignin and WAX® as binders and were employed in tests for the removal of lead ions from aqueous effluents.

The maximum removal of lead ions from the effluent reached approximately 88.36% within a 60-min timeframe. Analysis of the Freundlich and Langmuir isotherms revealed that the best data fit was achieved with the Freundlich isotherm ($R^2 = 0.98$). This was expected, particularly due to the addition of binders, with lignin playing a key role. Lignin not only provided strength to the pellets but also significantly contributed to the removal of Pb^{II}. The pseudo-second-order model described the kinetics of the process most accurately.

Pellets post-Pb^{II} adsorption were characterized, and the results indicated the presence of the metallic ion on the surface of the adsorbent. Pelletized palygorskite proved to be a highly promising material for removing lead ions from polluted water bodies. Additionally, this process allowed for the valorization of lignin, a byproduct of cellulose production.

SUPPLEMENTARY MATERIAL

Complementary material for this work (Figures 1S-5S) is available at http://quimicanova.sbq.org.br/, as a PDF file, with free access.

ACKNOWLEDGMENTS

We are grateful to CETEM for the laboratory structure, CAPES (PROEX), CNPq (405034/2023-7) and FAPERJ (E-26/211.688/2021) for financial assistance, and the mining company Mineração Coimbra Ltda. for providing the sample.

REFERENCES

1. Zhang, Y.; Duan, X.; *Water Sci. Technol.* **2020**, *81*, 1130. [Crossref]
2. Aendo, P.; Thongyuan, S.; Songserm, T.; Tulayakul, P.; *Sci. Total Environ.* **2019**, *689*, 215. [Crossref]
3. Barcelos, D. A.; Pontes, F. V. M.; Silva, F. A. N.; Castro, D. C.; Anjos, N. A. O.; Castilho, Z. C.; *J. Hazard. Mater.* **2020**, *397*, 122721. [Crossref]
4. Soliman, N. K.; Moustafa, A. F. I.; *J. Mater. Res. Technol.* **2020**, *9*, 10235. [Crossref]
5. Burakov, A. E.; Galunin, E. V.; Burakova, I. V.; Kucherova, A. E.; Agarwal, S.; Tkackev, A. G.; Gupta, V. K.; *Ecotoxicol. Environ. Saf.* **2018**, *148*, 702. [Crossref]
6. Churchman, G. J.; Gates, W. P.; Theng, B. K. G.; Yuan, G. In *Handbook of Clay Science*; Bergaya, F.; Theng, B. K. G.; Lagaly, G., eds.; Elsevier: Amsterdam, 2006, p. 625.
7. Uddin, M. K.; *Chem. Eng. J.* **2017**, *308*, 438. [Crossref]
8. Huang, R.; Lin, Q.; Zhong, Q.; Zhang, X. F.; Wen, X.; Luo, H.; *Arabian J. Chem.* **2020**, *13*, 4994. [Crossref]
9. Bertagnolli, C.; Kleinübing, S. J. D. A.; Silva, M. G. C.; *Appl. Clay Sci.* **2011**, *53*, 73. [Crossref]
10. Feng, Y.; Wang, Y.; Wang, Y.; Liu, S.; Jiang, J.; Cao, C.; Yao, J.; *J. Colloid Interface Sci.* **2017**, *502*, 52. [Crossref]
11. Potgieter, J. H.; Potgieter-Vermaak, S.; Kalibantonga, P. D.; *Miner. Eng.* **2006**, *19*, 463. [Crossref]
12. Chen, H.; Wang, A.; *J. Colloid Interface Sci.* **2007**, *307*, 309. [Crossref]
13. Zhang, T.; Wang, W.; Zhao, Y.; Bai, H.; Wen, T.; Kang, S.; Song, G.; Song, S.; Komarneni, S.; *Chem. Eng. J.* **2021**, *420*, 127574. [Crossref]
14. Simões, K. M. A.; Novo, B. L.; Marçano, G. B.; Silva, F. A. N. G.; Teixeira, V. G.; Afonso, J. C.; Bertolino, L. C.; Yokoyama, L.; *Rev. Mater.* **2023**, *27*, 1. [Crossref]
15. Litster, J.; Ennis, B.; *The Science and Engineering of Granulation Processes*, 2004th ed.; Springer: Dordrecht, 2004.
16. Ahir, A. A.; Mali, S. S.; Hajare, A. A.; Bhagwat, D. A.; Patrekar, P. V.; *Res. J. Pharm. Technol.* **2015**, *8*, 131. [Crossref]
17. Campos, A. R.; Fonseca, V. O. In *Tratamento de Minérios*; da Luz, A. B.; Sampaio, J. A.; França, S. C. A., eds.; CETEM/MCT: Rio de Janeiro, 2010, p. 705.
18. Simões, K. M. A.; Novo, B. L.; Felix, A. A. S.; Afonso, J. C.; Bertolino, L. C.; Silva, F. A. N. G. In *Characterization of Minerals, Metals and Materials*; Ikhmayies, S.; Li, B.; Carpenter, J. S.; Li, J.; Hwang, J. Y.; Monteiro, S. N.; Firrao, D.; Zhang, M.; Peng, Z.; Escobedo-Diaz, J.; Bai, C.; Kalay, Y. E.; Goswani, R.; Kim, J., eds.; Springer: California, 2017, p. 261. [Crossref]
19. Furlanetto, R. P. P.: *Estudo de Adsorção de Mercúrio em Palygorskitada Pelotizada da Região de Guadalupe-PI*; Trabalho de Conclusão de Curso, Universidade Federal do Rio de Janeiro, Rio de Janeiro, Brasil, 2018. [Link] accessed in August 2024
20. Araújo, C. S. T.; Almeida, I. L. S.; Rezende, H. C.; Marcionilio, S. M. L. O.; Léon, J. J. L.; Matos, T. N.; *Microchem. J.* **2018**, *137*, *348*. [Crossref]
21. Hall, K. R.; Eagleton, L. C.; Acrivos, A.; Vermeulen, T.; *Ind. Eng. Chem. Fundam.* **1966**, *5*, 212. [Crossref]
22. Doke, K. M.; Khan, E. M.; *Arabian J. Chem.* **2020**, *10*, 252. [Crossref]
23. Huang, R.; Yang, B.; Liu, Q.; Liu, Y.; *J. Appl. Polym. Sci.* **2014**, *131*, 39903. [Crossref]
24. Maciel, A. C. B.; Brandão, V. S.; Furlanetto, R. P. P.; Bertolino, L. C.; *XXVII Jornada de Iniciação Científica e III Jornada de Iniciação em Desenvolvimento Tecnológico e Inovação*; Rio de Janeiro, Brasil, 2019. [Link] accessed in August 2024
25. Pôssa, J. T.; Bertolino, L, C.; *Anuário do Instituto de Geociências* **2022**, *45*, 1. [Link] accessed in August 2024
26. Wang, W.; Wang, A. In *Nanomaterials from Clay Minerals*; Wang, W.; Wang, A., eds.; Elsevier: Amsterdam, 2019, p. 21. [Crossref]
27. Rodrigues, P. V.; da Silva, F. A. N. G.; Pontes, F. V. M.; Barbato, C. N.; Teixeira, V. G.; Assis, T. C.; Brandão, V. S.; Bertolino, L. C.; *Mater. Res.* **2023**, *26*, 1. [Crossref]
28. Lazghab, J.; Lenart, A.; *J. Food Eng.* **2005**, *157*, 79. [Crossref]
29. Ghaedi, M.; Ghezelbash, G. R.; Marahel, F.; Ehsanipour, S.; Najibi, A.; Soylak, M.; *Clean: Soil, Air, Water* **2010**, *38*, 877. [Crossref]
30. Demey, H.; Lapo, B.; Ruiz, M.; Fortuny, A.; Marchand, M.; Sastre, A. M.; *Polymers* **2018**, *10*, 204. [Crossref]
31. Vijayaraghavan, K.; Yun, Y.; *Biotechnol. Adv.* **2008**, *26*, 266. [Crossref]
32. McCabe, W. L.; Smith, J. C.; Harriott P.; *Unit Operations of Chemical Engineering*, 5th ed.; McGraw-Hill College: New York, 1993.
33. Oscik J.; *Adsorption*, 1st ed.; E. Horwood: Chichester, 1982.
34. Liu, Y.; Liu, Y.; *Sep. Purif. Technol.* **2008**, *61*, 229. [Crossref]
35. Esposito, A.; Pagnanelli, F.; Vegliò, F.; *Chem. Eng. Sci.* **2002**, *57*, 307. [Crossref]
36. Sparks, D. L.; *Environmental Soil Chemistry*, 2nd ed.; Academic Press: London, 2003.

37. Dada, A. O.; Olalekan, A. P.; Olatunya, A.; *IOSR J. Appl. Chem.* **2012**, *3*, 38. [Crossref]
38. Vijayaraghavan, K.; *Journal of Environment & Biotechnology Research* **2015**, *1*, 1.[Link] accessed in August 2024
39. Freitas, P. A. M, Iha, K.; Felinto, M. C. F. C.; Suárez-Iha, M. E. V.; *J. Colloid Interface Sci.* **2008**, *323*, 1. [Crossref]
40. Aguiar, M. R. M.; Novaes, A. C.; Guarino, A. W. S.; *Quim. Nova* **2002**, *25*, 1145. [Crossref]
41. Guo, X.; Zhang, S.; Shan, X. Q.; *J. Hazard. Mater.* **2008**, *151*, 134. [Crossref]
42. Chen, H.; Qu, X.; Liu, N.; Wang, S.; Chen, X.; Liu, S.; *Chem. Eng. Res. Des.* **2018**, *139*, 248. [Crossref]

This is an open-access article distributed under the terms of the Creative Commons Attribution License.